Computers & Graphics 122 (2024) 103958

Contents lists available at ScienceDirect

Computers & Graphics

journal homepage: www.elsevier.com/locate/cag

Special Section on STAG2023

Procedural generation of geometric patterns for thin shell fabrication

Elena Scandurra [a,b], Francesco Laccone [a,*], Luigi Malomo [a], Marco Callieri [a], Paolo Cignoni [a], Daniela Giorgi [a]

[a] Institute of Information Science and Technologies, National Research Council of Italy, via G. Moruzzi 1, 56126, Pisa, Italy
[b] Department of Computer Science, University of Pisa, Largo B. Pontecorvo 3, 56127, Pisa, Italy

ARTICLE INFO

Keywords:
Computational design
Digital fabrication
Shape modeling

ABSTRACT

This paper addresses the design of surface shells as assemblies of tileable, flat geometric patterns with predictable performance in response to mechanical stimuli. We design a family of tileable and fabricable patterns represented as triangle meshes, which can be assembled for creating surface tessellations. First, a regular recursive subdivision of the planar space generates different geometric configurations for candidate patterns, having interesting and varied aesthetic properties. Then, a refinement step addresses manufacturability by solving for non-manifold configurations and sharp angles that would produce disconnected or weak patterns. We devise a strategy for creating continuous variations on the geometry of individual patterns, in both aesthetics and behavior, to enrich the catalog of available designs. Finally, we simulate our patterns to evaluate their mechanical response when loaded in different scenarios targeting out-of-plane bending. Through a simple browsing interface, we show that our patterns span a variety of different bending behaviors. The result is a catalog of patterns with varied aesthetics and predefined mechanical behavior, to use for the direct design of mechanical metamaterials. To assess the feasibility of our design-to-fabricate approach, we show fabricated 3D objects with different curvatures, and compare physical and simulated experiments.

1. Introduction

Computational fabrication investigates the design and production of objects at different scales – from architecture to automotive and furniture – to speed up the classic design pipeline and overcome material, size, and geometric limitations. One of the opportunities opened up by computational fabrication is the design of *mechanical metamaterials* [1,2], a class of man-made structures whose mechanical properties are determined by the structure geometry. With metamaterials, one can fine-tune the mechanical properties of physical objects, even from a single fabrication material, by customizing their fine-scale geometry.

A sensible way of creating metamaterials is by using *patterns*, i.e. portions of space with a unique distribution of solid material and voids. Patterns can be assembled to create tiled surfaces, and the tiling of patterns with different geometries enables controlling the mechanical behavior of the resulting surface in response to mechanical stimuli, e.g. force, deformation, momentum [3]. A remarkable effect of pattern diversity is the creation of aesthetically pleasant surfaces; indeed, patterns have been extensively used in art and architecture, for example, for the roof of Louvre Abu Dhabi.

This paper aims to support the creation of metamaterials by tiling polygonal patterns. We make an initial step in this direction by designing and characterizing a catalog of geometric patterns that cover a wide range of mechanical behaviors, especially in terms of bending. Our patterns can be manufactured by 3D printing or laser-cutting and assembled to create aesthetically pleasing surface tilings. We demonstrate the potential of our pattern catalog by fabricating and testing different physical prototypes.

We cast pattern design as the combinatorial problem of locating solid material and voids over a surface. First, a regular recursive subdivision of the planar space generates different geometric configurations (Fig. 1(a)); then, a refinement step guarantees that patterns are fabricable and robust (Fig. 1(b)). We simulate the patterns to characterize their mechanical response under load (Fig. 1(c)), and present a simple browsing interface for exploring the design space, in terms of both aesthetics and behavior (Fig. 1(d)).

Differently from the majority of existing works, we target out-of-plane 3D deformations and evaluate the bending response of patterns in three different scenarios: Cantilever, Cylinder and Dome. Our simulation results show that the patterns exhibit a range of different mechanical properties and significantly expand the spectrum of possible deformations compared to solid structures. The user can select a pattern based on the desired stiffness and target deformation. Finally, different patterns can be easily manufactured as flat pieces and then assembled to form spatial assemblies (Fig. 1(e)).

* Corresponding author.
E-mail address: francesco.laccone@isti.cnr.it (F. Laccone).

https://doi.org/10.1016/j.cag.2024.103958
Received 28 February 2024; Received in revised form 9 May 2024; Accepted 4 June 2024
Available online 12 June 2024
0097-8493/© 2024 The Authors. Published by Elsevier Ltd. This is an open access article under the CC BY-NC-ND license (http://creativecommons.org/licenses/by-nc-nd/4.0/).

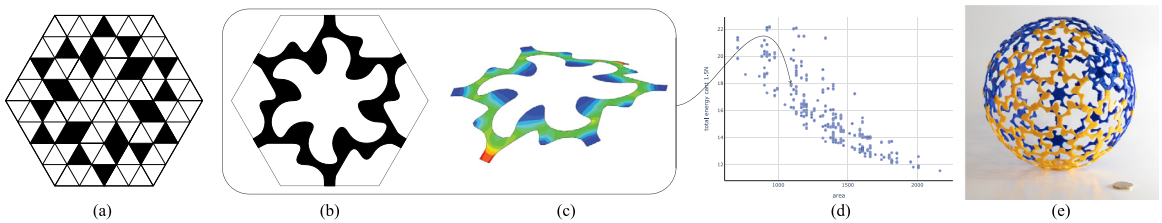

Fig. 1. Our pipeline, from pattern design to simulation and fabrication: (a) a polygonal pattern as a geometric configuration produced via regular recursive subdivision of the planar space, with black indicating solid material and white indicating void; (b) the corresponding fabricable pattern geometry after a refinement step; (c) the bending of the pattern under a simulated loading scenario; (d) the dot corresponding to the pattern in the browsing interface; (e) a sphere fabricated with two different patterns.

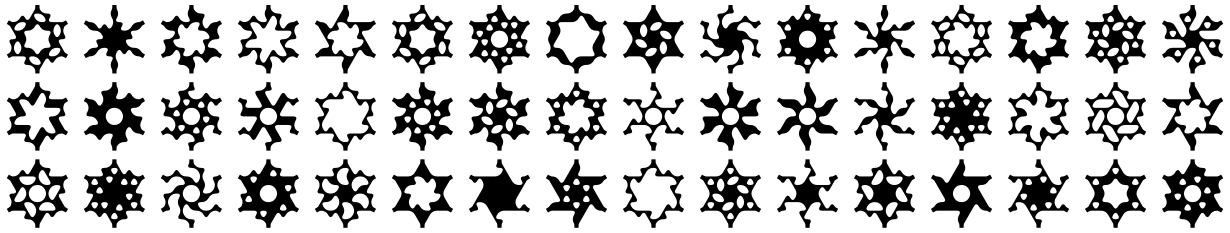

Fig. 2. A small subset of exchangeable, tileable, and connected patterns in our catalog.

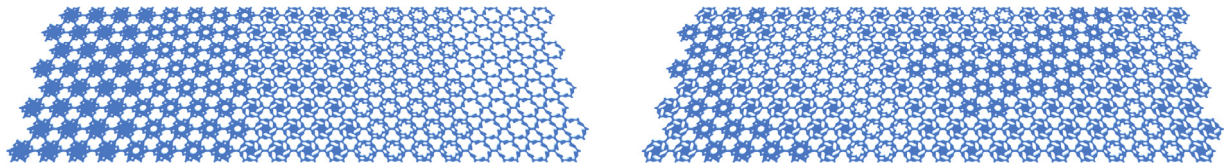

Fig. 3. Two examples of surface tessellations with different patterns.

The result is a catalog of patterns that can be employed to create surface tessellations for the direct design of metamaterials. Fig. 2 shows some example patterns, which span a variety of geometric and aesthetic properties. Fig. 3 shows example surfaces produced by assembling a subset of patterns in different configurations: adjacent patterns blend smoothly, and the whole metamaterial sheet has a seamless appearance.

2. Overview

Our aim is to design patterns that can perform as building blocks in composing larger macrostructures. We assume a polygonal and as-regular-as-possible tessellation for the target surface, in which as many tiles as possible have the same shape, for example, hexagons [4].

The patterns should be *tileable*, i.e. connect properly to adjacent patterns when placed in a tile, and *exchangeable*, i.e. fit into any region of the tessellation so that they can switch place, to expand the design space of mechanical structures achievable.

We start from the idea that every regular convex polygon can be decomposed into a fan of isosceles triangles emanating from its centroid; for example, a regular hexagon can be decomposed into a fan of six equilateral triangles. Therefore, we can create a polygon pattern by generating a sub-pattern in a triangular *slice* and then replicating it by rotational symmetry to fill any convex n-sided polygon. To generate different triangular slice patterns, we perform a combinatorial exploration of possible designs through recursive triangle subdivisions by considering all possible configurations of solid/void subtriangles at each subdivision step (Section 4). Fig. 4(a,b) shows example configurations for two subdivision steps. Once a triangular slice pattern has been designed, we generate the corresponding polygonal pattern by replicating the slice (Fig. 4(c,d)). The resulting rotational symmetric *pattern* embeds into the original polygon, can be easily adapted to polygons with a different number of edges by linearly mapping the base slice into every fan triangle, and is exchangeable by definition. Moreover, due to rotational symmetry, the positioning of a pattern is independent of possible rotations: this is convenient, as the mechanical properties of a structure composed of non-symmetric patterns would depend on the direction of each metamaterial unit inside the structure.

To guarantee connectedness and tileability, we define a filtering strategy to rule out slice configurations producing disconnected patterns and patterns that do not correctly connect to the boundaries. Finally, the last issues to address are fabricability and suitability for simulations. Indeed, the presence of non-manifold configurations and sharp angles in the pattern geometry would lead to disconnected or fragile patterns and possibly to singularities in computation. We address the problem by locally refining the geometry of patterns using quadratic rational Bézier curves (Section 5): we automatically identify problematic areas that would generate disconnected or fragile patterns and add material to produce fabricable geometries (Fig. 4(e)).

The result is a catalog of patterns that present high variability in terms of shape, aesthetics, and mechanical properties to support applications in metamaterial design. According to the combinatorial strategy outlined above, the amount of patterns that constitute the catalog depends on the number of subdivision steps performed in the combinatorial exploration phase. This paper considers two subdivision steps: the combinatorial exploration phase produces 65535 geometries; after the filtering procedure, 430 exchangeable, connected, tileable patterns are left (including mirrored patterns produced by symmetrical triangular slices).

Of course, larger catalogs could be obtained by performing more subdivision steps. However, this would cause combinatorial expansion. To solve this issue, we introduce a strategy to augment the gamut of mechanical and aesthetic properties of our pattern catalog while leaving the combinatorial generation process unchanged. The idea is to continuously vary the geometry of existing patterns via perturbation of the spatial position of vertices in the subdivided triangle slice, thus

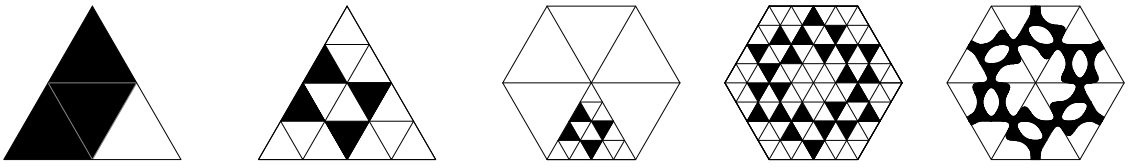

Fig. 4. The steps in our pipeline. We consider different solid/void subtriangles' configurations in a triangular slice at multiple subdivision steps (a,b). The triangle slice is embedded into a polygon, a hexagon, in this example (c). A polygonal pattern is generated by replicating the triangle slice via rotational symmetry (d). To get the final fabricable patterns, we add solid material around predefined vertices using quadratic rational Bézier curves and a connectivity-preserving logic (e). [5].

generating possibly infinite, spatially-graded variations in aesthetics and behavior. This step enriches the expressiveness of the design space while avoiding combinatorial explosion (Section 6).

Our contribution is a simple yet elegant method to produce aesthetically pleasant patterns at a controllable scale. This work was originally presented at STAG 2023, International Conference on Smart Tools and Applications in Graphics. With respect to the conference paper [5], a first novel contribution is a strategy for enriching the design space by adding possibly infinitely many patterns to the original catalog via perturbation of the vertices of the initial planar space subdivision (Section 6). Then, we add experiments on two 3D physical prototypes to validate quantitatively our proposal. We 3D print two flat tilings of patterns, apply loads, and validate the accuracy of simulations by 3D scanning the deformed fabricated models and comparing the scanned and the simulated object (Section 10.2). The agreement between the physical and the simulated experiment demonstrates the accuracy and the potential of our design-to-fabrication pipeline.

3. Related work

Our contribution fits within a large and thriving area of research in computer graphics on fabrication-aware design. We summarize in what follows the relevant state of the art on fabrication and design of patterns and metamaterials.

3.1. Computational design and fabrication of patterns

Polygonal tilings have been studied for a long time in mathematics [6,7] and are used in particular for their intriguing aesthetics. Their computational design has a long history in computer graphics [8–10]. Lately, discrete tiles were also employed to approximate a desired 3D shape by creating ornamental motifs [11–13]. Stylized surfaces exploit a specific fabrication technique or a style and reinterpret a target shape in an artistic manner while preserving its global geometric features [14].

Pattern design complexity increases when used for architecture or engineering intents at all scales since structural properties need to be carefully considered. The work [15] proposes a computational method to design variously-shaped curve networks on the object surface. Conversely, in a subtracting fashion, artistic cutouts can be carved on a shell surface with a constraint of global stability of the shape as in [16]. Patterns can also affect the kinematics of an object. In the presence of actuation, the 3D printed stripes in [17] allow compliant mechanisms of stretchable membranes. In [18], a pattern of cuts on given material sheets is inversely designed to control a kirigami shape-morphing.

3.2. Metamaterials

Metamaterials are artificially conceived materials that cannot be found in nature. Their properties are determined by the inner distribution of solids and voids rather than their material properties at the atomic level. The behavior control occurs at the meta- (or meso-) scale level, while the effects are observed at the macro-scale, i.e. in terms of deformation, stress, energy [3,19,20]. The synthesized behavior obtained so far via metamaterials include, for instance, exotic bulk-to-shear-moduli ratios (named auxetic materials) [21,22], controllable shape deformations [2,23,24], enhanced mechanical response [25,26].

Metamaterials are created out of a repetition of patterns [27–29], in which the unit cells are often extremely tailored, possibly determining an unusual appearance of the assembly. Indeed, the interplay between mechanical behavior and aesthetics gives birth to new challenges related to the joint design of mechanical properties and appearance.

3.3. Model description and optimization

Physical simulation has long been used in computer graphics for virtual animations. More recently, the rising importance of computational fabrication called for accurate simulations of material behavior. As regular finite elements require intense computation, several reduced models have been adopted to describe the mechanical behavior of metamaterials for in-plane, bending, static, or dynamic behavior. Despite the deep knowledge in material science on how to model the macro-behavior of micro-structures, novel design theories, and fabrication technologies, such as 3D printing, give birth to interesting and unusual deformation modes, which require updated and efficient descriptions [30]. Homogenization is a widespread effective theory that maps complex and non-homogeneous assembly to a coarser equivalent behavior at the macro-scale [31]. A viable alternative is a reduced-order simulation, where the single metamaterial cell is replaced, for instance, by a less intensive structure with simple or fewer elements [32,33]. Inverse design problems face the creation of tailored metamaterials to conform locally to particular shapes or mechanical specifications, and take advantage of reduced models to optimally place bespoke units within an ideal voxel domain. This problem relates to topology optimization, which investigates how to distribute solid material within a target volume to maximize a given structural objective [34–36].

3.4. Comparison with relevant competitors

Our method deals with generating flat patterns tiled on a surface. Flat pieces are practical since they can be easily transported and manufactured in different sizes with different fabrication techniques. In [37] an input surface is approximated by using flat parameterized spiraling patterns to produce small-scale and architectural-scale objects [38,39]. However, the pattern geometry is constrained to a four-arm spiral pattern, and the reduced representation proposed only applies to that specific type of pattern. In contrast, our goal is to produce a broad family of patterns, providing significant variability in aesthetics and mechanical properties.

Tozoni et al. [40] created a set of parametric rhombic microstructures with a continuous mapping between geometric parameters and mechanical properties. Similarly, Martinez et al. [3] generate 2D tiled geometries from Voronoi diagrams of regular lattices under star-shaped distance functions. Their microstructures can be interpolated to vary their mechanical properties smoothly. To assess the mechanical behavior of pattern arrangements, the authors relied on homogenization [41]. However, these approaches apply only to in-plane scenarios, where the patterns have few deformation modes, and it is easier to map them to

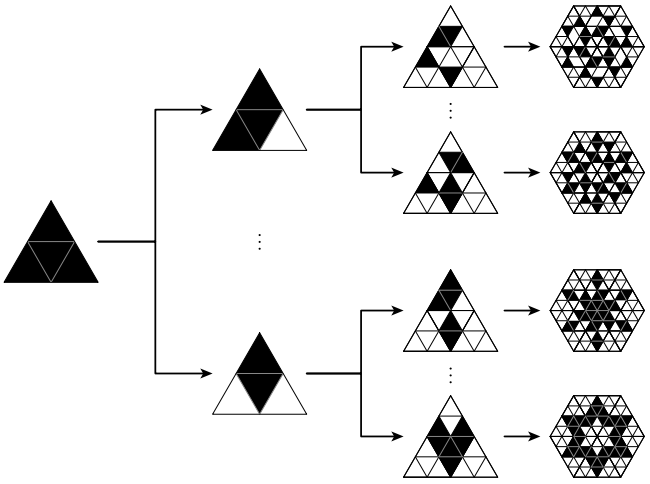

Fig. 5. From left to right: the solid triangle; two possible solid/void configurations produced after a first subdivision step; four possible solid/void configurations produced after a second subdivision step; the polygonal patterns they generate. [5].

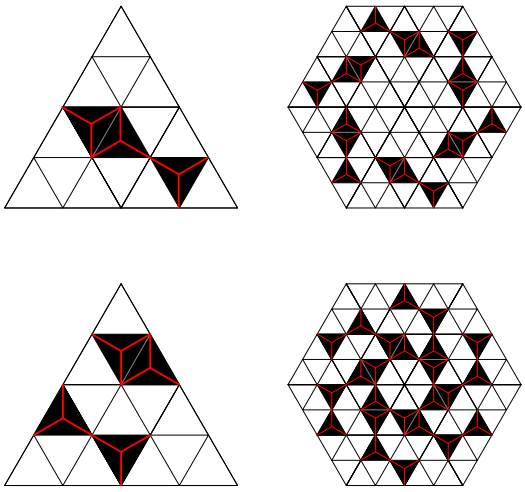

Fig. 6. (Top) A connected slice that generates a disconnected solid pattern; (bottom) a disconnected slice that generates a connected solid pattern.

a simpler mechanical model. In contrast, in this work we target out-of-plane deformation of flat patterns, and we run *a posteriori* simulations so that the user can explore the space of all possible behaviors and select the most suitable pattern based on its response. Indeed, homogenizing a generic 3D mechanical behavior is still an open research question [42], which is beyond the scope of this paper.

4. Pattern design via iterative space subdivision

4.1. From slices to patterns

We start by generating a geometry that can fit into any isosceles triangle, called a slice. More formally, a *slice* is a regular triangulation of a base triangle; every face has a label that is either 1 or 0. Label 1 indicates solid regions (i.e. regions filled with material), while label 0 indicates void regions.

Fig. 5 illustrates the subdivision and slice generation process. To list the set of possible triangle slices, we perform a combinatorial exploration of the space of possible slices through regular recursive subdivision of a base triangle (1 to 4). We start from the solid triangle, representing the full slice (Fig. 5(left)), and subdivide it into four sub-triangles. We then consider all possible configurations of solids/voids, adopting a subtractive approach and removing triangle areas. We exclude the all-void configuration, as we require that a solid triangle produces at least one solid subtriangle. Each slice can be visualized by coloring the solid and void subtriangles in black and white, respectively. For each configuration, we further subdivide each triangle into four as above. Again, following a subtractive approach, a solid triangle will generate all but one (15) configurations of solids/voids, while void triangles produce only the void configuration (Fig. 5(middle)).

The process can be recursively applied, thus producing a tree of configurations. At the nth step of recursion, the base triangle is subdivided into 4^n subtriangles, with at least a solid one. This corresponds to $2^{4^n}-1$ possible slices. This work considers two recursion steps corresponding to $2^{16}-1$ possible slice geometries. If we define an ordering of the faces of the triangulation, we can encode the sequence of solids/voids in a bit-string that uniquely defines the slice.

Replicating a slice by rotational symmetry generates a triangulation of a regular hexagon with labeled faces (Fig. 5(right)). We refer to this new labeled triangulation as a *pattern*. We encode the geometry of each pattern by V, F, c, where V is the list of vertices, F is the list of triangular faces and c is a binary vector of size $|F|$ expressing whether the ith element maps by rotational symmetry to a solid (or void) triangle of the generating slice. In analogy to the above, we call *solid pattern* the subcomplex induced by the solid triangles of a pattern. Each solid pattern is identified by a couple $\widetilde{V}, \widetilde{F}$, where $\widetilde{F}$ is the subset of F determined by faces that are labeled by 1 in c.

4.2. Exchangeability, connectedness, tileability

By construction, all slices generate patterns that can be embedded into any regular polygon; hence, exchangeability is guaranteed. Unfortunately, not all patterns are suitable for producing mechanical metamaterials. Indeed, triangle slices may produce solid patterns that consist of separate components; therefore, we need to select only slices that generate connected solid patterns. Furthermore, we enforce tileability so that patterns embedded into adjacent polygons connect correctly. Tileability and connectedness together ensure that, if a target surface is connected, it remains connected if tessellated using any subset of patterns. The following paragraphs detail our filtering strategy to select slices that produce connected and tileable patterns.

Connectedness. In our analysis, we have observed that disconnected slices do not necessarily imply disconnected patterns, and vice versa, as illustrated in Fig. 6. Therefore, relying solely on the connectivity of a single slice is not sufficient to assess the overall connectivity of the generated pattern. We model the connectivity of the whole pattern using a graph G, which encodes the adjacency between the faces of the generated solid structure. We model each face of the solid pattern triangulation as a node (referred to as face node), accompanied by its three vertices (vertex nodes). All face nodes are connected to their vertex nodes (red edges in Fig. 6). The graph thus defined is a simplicial complex of dimension 1, where the link of a vertex node is the discrete set of face nodes associated with the triangles containing that vertex. It holds that a slice produces a connected solid pattern if and only if the graph G is connected.

Given the consistent topology of the base slice across the triangle fan, one might be tempted to construct the graph G using a single slice and connecting the nodes on the left side to their corresponding nodes on the right side.

However, this approach proves insufficient for capturing the connectivity of cyclic structures. As a counterexample, this approach would incorrectly identify the pattern generated by the triangular slice shown in Fig. 7 as connected. The solution is to generate the graph G on two adjacent slices, with their open sides connected at corresponding nodes. This method ensures a comprehensive evaluation of both intra- and inter-slice connectivity, regardless of the number of triangles comprising the pattern.

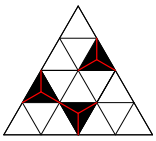

Fig. 7. Connectedness failure case.

Tileability. Having defined a criterion to select slices that correspond to connected solid patterns, we must deal with the problem of assembling solid patterns to produce a connected structure. Patterns must connect along the boundaries of the polygon. Therefore, we need to restrict to solid patterns that touch the boundary of the polygon. Obviously, this is not a sufficient condition: if two adjacent solid patterns are connected to disjoint points on the polygon boundary, they still fail to connect to one another (Fig. 8(a)). Additionally, we have to prevent patterns from only partially connecting along the polygon boundary (Fig. 8(b)), which would complexify the mechanical interaction of adjacent solid patterns.

To ensure proper connection, we impose the condition that the intersection between a solid pattern and a polygon edge must be symmetric with respect to the midpoint of the polygon edge. We say that two patterns *properly connect* if they induce two solid patterns such that the edges and vertices that lie on the common polygon boundary coincide (Fig. 8(c)). A family of patterns that properly connect to each other is tileable and is suited for mechanical simulations. To avoid complex behaviors in mechanical interactions of adjacent solid patterns, we restrict to patterns that connect exclusively on the open edge of the polygon, thus excluding the case of three (or more) solid patterns sharing a polygon vertex. In particular, we select solid patterns that connect to the boundary of the polygon exactly by the midpoint of its edges. To perform this selection, we simply check that all faces of the boundary edge of a slice are void except the middle triangle (e.g., Fig. 4(c)).

The solid patterns are then modified to produce a metamaterial that is fabricable, with a *filleting* procedure described in the next Section.

5. Addressing aesthetics and manufacturability via vertex filleting

Thus far, we have defined conditions for slices to produce solid patterns that are tileable, exchangeable, and connected. However, we need some post-processing to generate fabricable solid patterns with a proper structure and suited to perform mechanical simulations. Indeed, slices with non-manifold vertices produce solid patterns that, when manufactured, would result in either a disconnected or weak object. Similarly, the connections between patterns should be robust enough. Finally, the presence of sharp angles can lead to inaccuracies in the mechanical simulation of the pattern and also affect the aesthetics of patterns. Fig. 9(a) shows problematic vertices in a solid pattern: non-manifold vertices (green dots), sharp angles (blue dots), and interface vertices that connect two patterns (red dots). To address these issues, we locally refine the shape of the solid pattern around problematic vertices by adding or removing solid material according to the configuration of the star of vertices. In other words, we edit patterns so that they are represented by a 2-dimensional piecewise-linear (PL) manifold mesh with boundary, where the boundary PL-approximates smooth curves (Fig. 9(c)).

The first step is to identify problematic vertices. This step can be performed by analyzing the link of each vertex in a solid pattern. Non-manifold vertices are identified as vertices whose link is disconnected. Sharp angles are identified as vertices whose link is connected and made of a number of edges different than three or six. Interface vertices are identified as vertices that lie on the polygon edge. Fig. 10(top row) shows the set of possible configurations of solid/void triangles in the star of a non-manifold vertex, up to rotations; Fig. 11(top row) shows the set of possible configurations of solid/void triangles in the star of a vertex corresponding to a sharp angle, up to rotations. Lastly, Fig. 12(left) shows the configuration for interface vertices, up to rotations.

The idea is to locally refine the mesh representing the pattern around a problematic vertex by adding vertices in its open star. The vertices approximate quadratic rational Bézier curves, whose control polygons are pairs of edges incident to the problematic vertex and shared by a solid and void face. The pairs of edges defining the control points are chosen to preserve the connectedness of the pattern. The weights for the control points are assigned by following two strategies, depending on whether the vertex lies in the interior of the polygon or on one of its edges. Therefore, we create a look-up table with all problematic vertex configurations and the corresponding filleting strategy. If the vertex is non-manifold or represents a sharp angle, we assign the same weight to all the control points, thus producing a quadratic Bézier curve. The resulting curves are shown in Fig. 10(bottom row) and Fig. 11(bottom row). If, instead, the vertex lies on a polygon edge, the curves are defined considering that, once the patterns are connected, the vertex produces a non-manifold configuration already considered in the previous cases (Fig. 12). In this case, we assign different weights to the control points to produce a stiff connection among patterns. In this paper, we consider $(1, 0.2, 1)$ as the weight vector for control points, where 0.2 is assigned to the interface vertex and 1 is assigned to its adjacent control points. The resulting curve is shown in Fig. 12(right). This choice of weights ensures that the patterns can be simulated and properly fabricated without altering their aesthetics.

One issue to solve is that different orderings in performing the filleting of vertices could produce different results, as the filleting affects the star of vertices. To this end, we perform a mesh subdivision step to guarantee that local modifications around each vertex are independent of the ordering in which they are applied. Formally, let $\mathcal{L}$ be the set of indices of problematic vertices in the mesh $\mathcal{M} = (V, F)$ representing the pattern. We perform a refinement step by further subdividing the triangles into four sub-triangles (Fig. 9(b)). This step produces a new mesh $\hat{\mathcal{M}} = (\hat{V}, \hat{F})$ and a corresponding set $\hat{\mathcal{L}}$ of updated indices of vertices to process. In the refined mesh $\hat{\mathcal{M}}$, the vertices in $\hat{\mathcal{L}}$ will necessarily belong to different faces; in particular, their open stars will be pairwise disjoint. Therefore, the local modification of the open star of vertices in $\hat{\mathcal{L}}$ yields results that are independent of the order of vertex processing.

To locate the set of vertices B approximating the boundary curves, we employ the generalized De Casteljau algorithm for rational Bézier curves [43]. We update the set of vertices $\hat{V}$ by adding the vertices in B and the set of mesh faces $\hat{F}$ accordingly. It is important to note that, thanks to the subdivision step yielding $\hat{M}$, the rational Bézier curves are locally defined so that geometric continuity of the tangent vector is globally ensured (Fig. 9(c)). Finally, if $\widetilde{\mathcal{M}}$ is the mesh representing the solid pattern induced by $\hat{\mathcal{M}}$, we isotropically remesh $\widetilde{\mathcal{M}}$, before simulating its mechanical behavior.

6. Augmenting the design space via perturbations of the base geometry

The patterns generated by our method exhibit a discrete nature, characterized by a limited number of variations determined by the triangle subdivision steps. This discrete nature limits the number and diversity of available patterns by design. Indeed, with two subdivision steps, the combinatorial exploration and the subsequent filtering phase produce a discrete set of 430 different geometries.

While increasing the number of subdivision steps would increase the number of patterns, it would also lead to a costly combinatorial expansion. Therefore, to enhance the expressiveness of patterns within the same discrete combinatorial framework, we introduce a method to obtain continuous shape variations without altering the topology of patterns. We spatially displace the positions of the vertices in the

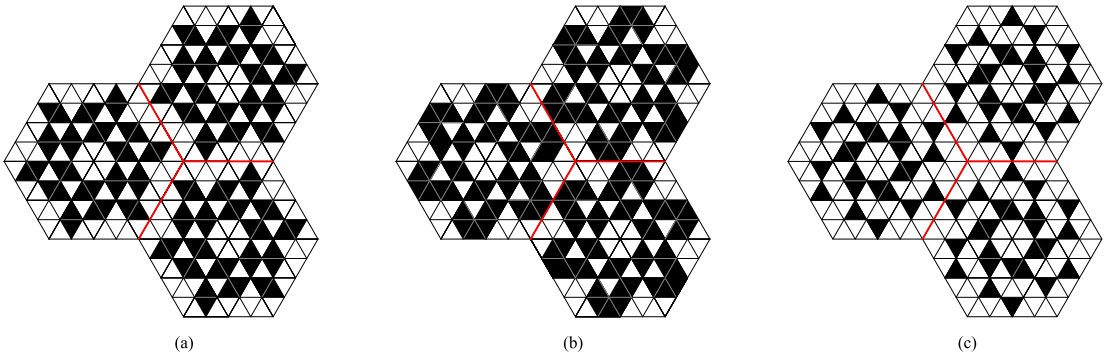

Fig. 8. Sample tiling of a single pattern in a hexagonal tessellation: (a) a solid pattern that fails to connect; (b) a solid pattern that fails to connect properly; (c) a solid pattern that properly connects. [5].

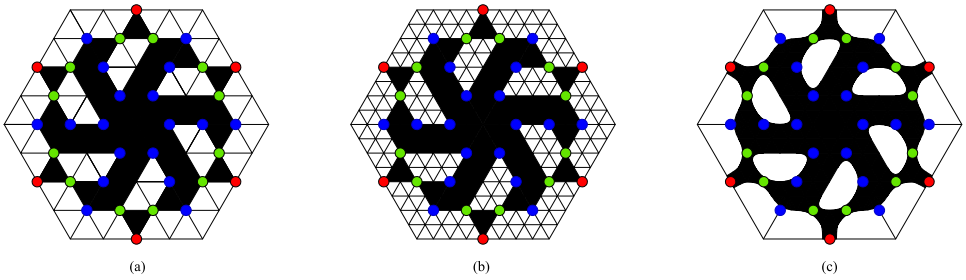

Fig. 9. (a) A pattern as a simplicial 2-complex with colored faces. The sub-complex generated by black faces is the solid pattern, which has non-manifold vertices (green dots), vertices identifying sharp angles (blue dots), and interface vertices connecting different patterns (red dots); (b) Mesh refinement before the filleting procedure around problematic vertices; (c) filleted pattern, with boundaries that approximate smooth curves [5].

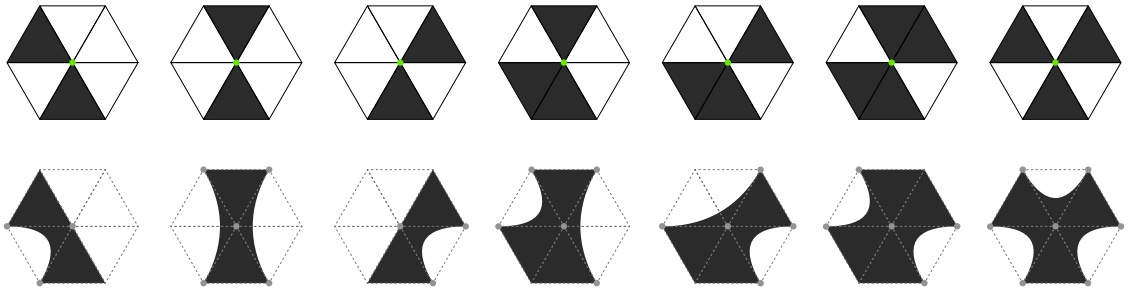

Fig. 10. All possible configurations of solid/void triangles in the star of non-manifold vertices (top row) and the corresponding filleting strategies (bottom row). Gray dots indicate Bézier control points.

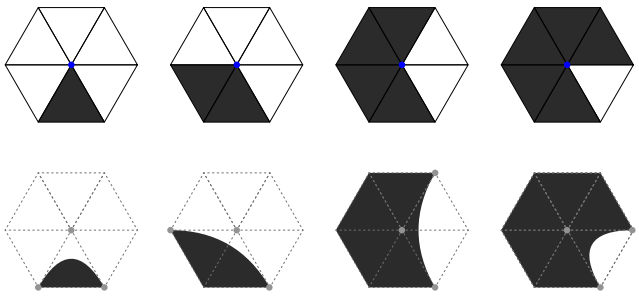

Fig. 11. All possible configurations of solid/void triangles in the star of vertices at sharp angles (top row) and the corresponding filleting strategies (bottom row). Gray dots indicate Bézier control points.

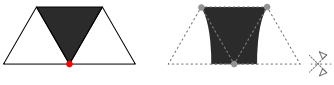

Fig. 12. Filleting interface vertices that lie on the polygon edge. Gray dots indicate Bézier control points.

triangle slice at the second subdivision step while keeping the solid pattern generation process unchanged. By continuously moving the position of vertices in the triangle slice, each of the 430 patterns possibly yields an infinite spectrum of shape variations.

Fig. 13 illustrates 16 example shape variations in the geometry of the base triangle (first and fourth columns) and the corresponding 16 shape variations generated for two distinct base patterns. It can be observed how different geometries in the triangle slice result in noticeable variations in the corresponding patterns. Remarkably, as we will show in the experimental section, as the variations proposed influence the pattern geometry continuously, they result in a spectrum of mechanically-varying properties for each pattern. Therefore, the design space is largely enriched, both in terms of aesthetics and behavior.

To ensure tileability, we only allow moving the vertices that do not belong to the polygon edge and the interface triangle. Indeed, moving the vertices at the interface between patterns could produce non-matching shapes while connecting different patterns.

7. Testing and fabrication experimental setup

Our pipeline is implemented in Python, using the libraries libIGL [44] and PyMeshLab [45] to manipulate 3D meshes. We perform

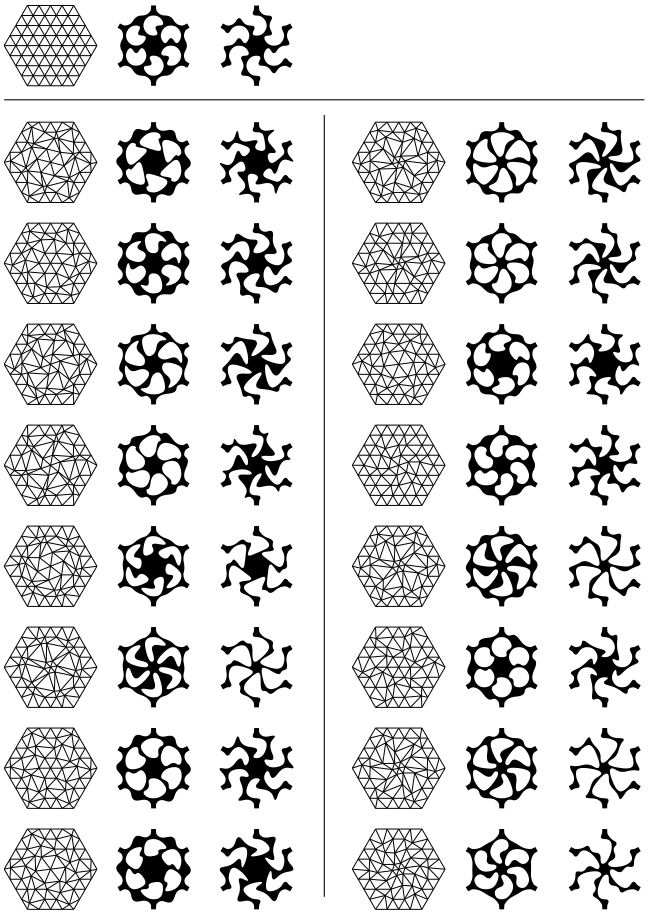

Fig. 13. Example shape variations on two patterns in our catalog. Top row: the original regular geometry of the triangle slice (repeated to form a hexagon) and the corresponding patterns. First and fourth columns: variations in the geometry of the triangulation, obtained via displacing the spatial positions of vertices. The other columns show the corresponding variations in the generated patterns.

simulations to characterize the mechanical response of patterns. We consider three different loading scenarios (Cantilever, Cylinder and Dome), and analyze the simulation results in detail for two different patterns (Section 8). We use the commercial Finite Element software Abaqus [46] to perform the simulations. Before solving the models, we remesh the patterns with an isotropic triangulation using a target edge length of 2mm. The triangle mesh is converted into S3 small-strain shell finite elements to perform a nonlinear static analysis with large displacements. A linear elastic isotropic material model is adopted, simulating a common 3D printed PLA material with density of 1.23 g/cm^3, Young's modulus of $E = 1.0$ GPa, and Poisson ratio 0.3.

To support the user in the navigation of the design space, we implemented a browsing interface that allows the exploration of the catalog of patterns in terms of mechanical properties and aesthetics (Section 9).

To validate our design-to-fabrication pipeline, we fabricate different physical structures and compare their behavior with respect to calibrated simulation results (Section 10). The structures are fabricated with an Ultimaker S5 3D printer using PLA material. The structures involved in the physical tests were measured using a metrology structured-light 3D scanner (GOM ATOS 5M).

For both simulation and physical fabrication, patterns are installed in a regular hexagon with edge length equal to 3.6 cm, and thickness equal to 0.2 cm.

8. Structural simulation results

We tested the dataset of 430 patterns against three standard scenarios that cover a sufficient range of deformations. These scenarios mobilize the main ways of loading 2D thin plates in the out-of-plane direction, which induces 3D bending. While characterizing a mechanical metamaterial for in-plane deformation or loading is a widespread topic, exploring its bending behavior in 3D is a novel subject. Simulation results reveal that our patterns exhibit a variety of deformations, expanding the range of deformations obtainable with solid, non-patterned materials.

We showcase two patterns with different geometric features and void/solid distribution to describe the three scenarios and to prove the high variability of their structural response. The first pattern has rotational symmetry and has a small area located peripherally. The second pattern has XY symmetry and has a dense, centered area (Fig. 14).

In our first scenario, the pattern is cantilevering from one interface extreme and is submitted to an out-of-plane force of $F_z = 1.5$ N on the opposite extremity. The fixed extreme has fully fixed nodes. We aim at simulating the elastic shape of the patterns. The results in Fig. 14(a) show the deformed shape of the patterns in the Cantilever scenario with a superimposed color map of the strain energy per finite element. The patterns initially lay on the XY plane. As expected, the structures show a diverse and complex behavior even for this simple scenario. The first pattern (Fig. 14(a,top)) has non-symmetric deformation field and uneven distribution of strain energy, as demonstrated by the non-symmetric colors in the map. For the same load, it attains higher deformation than the second pattern (Fig. 14(a bottom)). The load path from the application point to the support is long in the first case, so the forces flows along the entire pattern. Besides its larger area, the second pattern is also more efficient, providing a more direct load path. Moreover, its stress and deformation are XY symmetric. A solid hexagon would behave similarly to the bottom pattern but with a stiffer response. Instead, it would be impossible to compare the top pattern with a solid hexagon.

In our second scenario (Fig. 14(b)), the patterns are deformed to assume a cylindrical shape. In this setup, we use pin joints on one extreme to fix X, Y, and Z translations and roller joints on the opposite extreme to fix only Z translations. Then, we apply opposite bending moment $M_x = 50$ Nmm on both extremes to shrink the Y distance between them (the rollers slide towards the pins) while inflating the shape. The results show a different stiffness of the patterns as demonstrated by the displacement field and the strain energies. While the most prominent utilization of the structural material is at the supports as expected, the less dense pattern (Fig. 14(b,top)) is also characterized by localized high-energy areas when the width of patterns is reduced. Instead, when the width is larger, parts of the patterns are unused and dangling, so they remain almost flat. The color map has rotational symmetry. The pattern in Fig. 14(b,bottom) has a very low XY-symmetric deformation and can be compared with a solid hexagon tile.

Our third scenario simulates double curvature (Fig. 14(c). Here, one extreme has a pin joint (X, Y, Z fixed translations), while all the other extremities have roller supports, so they are constrained to be on the XY plane but can slide on it. We applied bending moments $M = 100$ Nmm, whose axes are aligned with the edge of each extreme, to have a blow-up effect that makes the shape similar to a Dome. In this scenario, bending forces applied with different axes induce a complex state of internal forces acting in the pattern. Therefore, the strain energy is affected by the straight bending along the supports and by in-plane bending elsewhere. In particular, the pattern in Fig. 14(c,top) suffers from stress concentrations in small-width areas due to in-plane bending. The pattern has a large deformation and consequently attains high energy. Instead, the pattern in Fig. 14(c,bottom), is much more efficient because it has larger and centered structural material to face the equilibrium of all the radial forces coming from the extremes. Moreover, its 'star points' are affected only by straight bending.

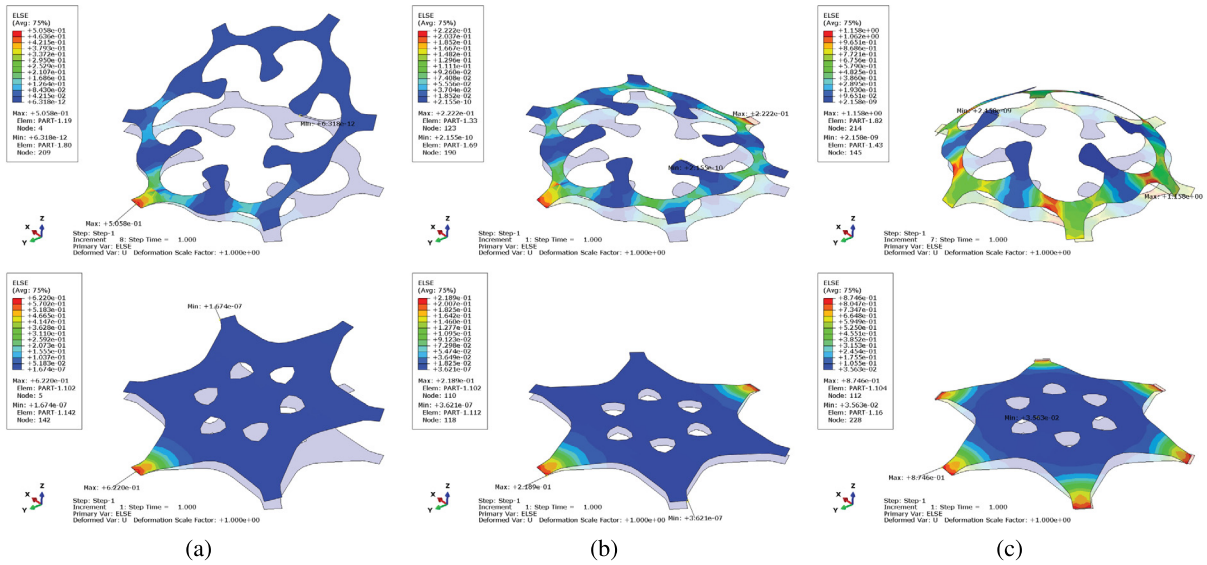

Fig. 14. Mechanical analysis results: 'Cantilever' (a), 'Cylinder' (b), and 'Dome' (c) simulation cases shown for two patterns (top and bottom). The strain energy is color-mapped on the deformed pattern..

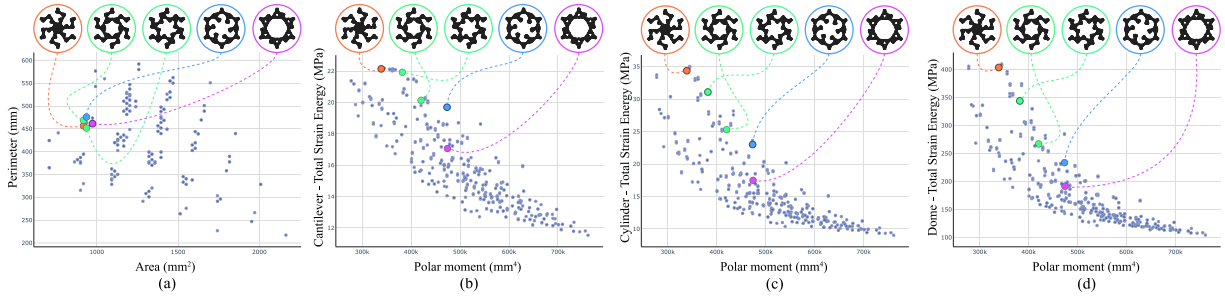

Fig. 15. Scatter plots representing the family of patterns and the relation between geometric and mechanical characteristics. Each dot represents a pattern. (a) A first cluster of patterns having similar geometric features, highlighted in color; scatter plot according to perimeter and area. (b,c,d) Scatter plots for the three different simulation scenarios, according to polar moment and total strain energy [5].

9. Exploring the design space

From the user's perspective, finding patterns that exhibit a certain aesthetics and simultaneously target a mechanical behavior is not easy, being the relation between geometry and mechanical performance often not intuitive. Therefore, we designed a simple browsing interface that enables the exploration of the design space, in terms of both aesthetics and behavior, using scatterplots. The dots are patterns, while x and y coordinates indicate geometric and mechanical parameters (area, perimeter, and their normalized ratio, polar moment, total strain energy).

The geometric complexity of the patterns makes the mechanical characterization a challenging task since each pattern can be strongly affected by local phenomena, i.e., excessive deformation, stress concentration, or even failure. Nevertheless, in the early design phase, it is convenient to describe a pattern's mechanical behavior by means of a high-level single parameter so that the user can select a subset of patterns to employ in a tiled configuration. Internal forces among patterns spread out based on their stiffness, and, to have equilibrium, all patterns shall have a similar energy level. Therefore, we show examples of navigating the design space of our patterns while using the total strain energy of a pattern in each scenario.

Figs. 15 and 16 report examples of plots, which can be explored in our design interface. We use perimeter (mm) and area (mm^2) to describe the geometric features of the patterns. Consequently, clusters in the scatter plot perimeter-area highlight patterns that are uniform from an aesthetic perspective. Identifying clusters is quite simple due to the discrete nature of the generation process of removing one triangle at a time. We use the polar moment of area as an additional parameter to plot the values. The polar moment has a geometric meaning and characterizes the distribution of the area with respect to the center of the hexagon. For the same area, patterns with peripheral distribution have higher polar moments. Additionally, the polar moment has a mechanical meaning in that it describes the attitude of a body to resist torsion. Moreover, the polar moment is the sum of the two moments of area, namely the description of the resistance to bending. In general, the higher the polar moment, the stiffer the pattern. Finally, this parameter is simple to compute and can be obtained from geometry only.

In Fig. 15 we select patterns from a geometric cluster. In plots (b), (c), and (d), these patterns reveal a very different mechanical behavior, as shown by the colored dots in the scatter plot. The importance of the strain energy can be observed by looking at the patterns highlighted in blue and magenta: even if they have similar area, perimeter, and polar moment, the magenta one is more efficient and does not suffer from underused parts (dangling components discussed in the previous Section). In particular, the strain energy values for the three scenarios are 17.06, 17.49 and 191.61 MPa for the pattern highlighted in magenta, and 19.69, 23.01 and 233.60 MPa for the pattern highlighted in blue.

In Fig. 16, we select a different cluster of patterns having higher area and lower perimeter. Therefore, they are compact and stiffer on average than the patterns in the previous cluster. The same discussion on the dispersion of energy data also holds in the present case. However, it is

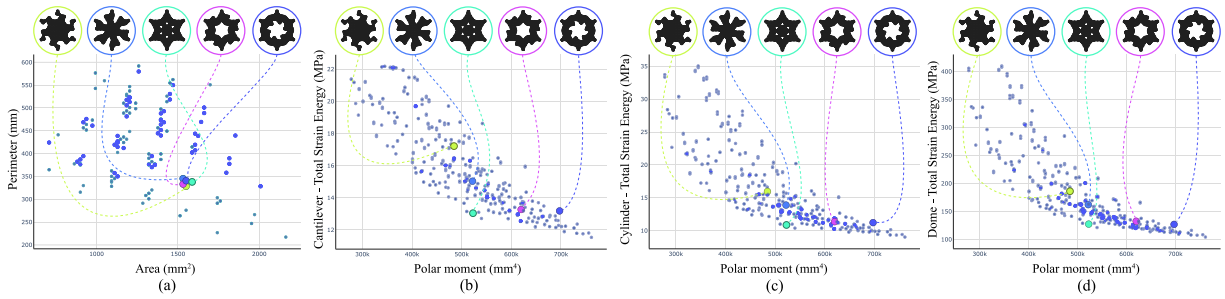

Fig. 16. Scatter plots representing the family of patterns and the relation between geometric and mechanical characteristics. Each dot represents a pattern. (a) A second cluster of patterns having similar geometric features, highlighted in color; scatter plot according to perimeter and area. (b,c,d) Scatter plots for the three different simulation scenarios, according to polar moment and total strain energy [5].

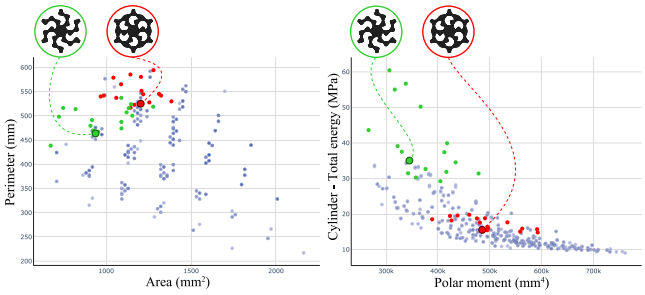

Fig. 17. Scatter plots showing how the variations in the pattern geometries obtained via vertex displacements (green and red dots) reflect in the gamut of available aesthetic (left) and mechanical (right) properties..

important to observe that the mechanical performance is also scenario-dependent. Indeed, the first pattern of the present cluster (lime green in Fig. 16) has total strain energy similar to the last pattern in the previous cluster (magenta in Fig. 15) in the case of Cantilever and Dome (17.21 and 186.13 *vs* 17.06 and 191.61 MPa). At the same time, this value is different in the Cylinder scenario (15.95 *vs* 17.49 MPa).

The scatterplots above show how users can explore the design space spanned by the 430 patterns generated by our combinatorial strategy. As observed in Section 6, the design space can be enriched by considering variations on each of the 430 patterns, by altering the position of vertices in the triangle slice that generates the pattern at hand. Fig. 17 shows how the patterns generated by the 16 example variations in Fig. 13 are positioned in the scatterplots for perimeter/area and for strain energy/polar moment in the cantilever scenario, for two example patterns. It can be observed that the variations largely enrich the gamut of shapes available, as well as the gamut of mechanical behaviors available to the users. Even though we have only shown a handful of example variations, the number of variations is possibly infinite and continuously depends on the amount of vertex displacements; therefore, the variations result in a spectrum of mechanically varying properties for each pattern. These continuous variations open up the possibility to largely densify the design space of our patterns.

The features described above enable the combining of patterns based on the visual effect a designer may want to achieve. However, they also remark on the centrality of the intended use of a tessellated plane since only certain combinations of patterns are effective for a given curvature or target shape, as shown by the fabricated examples in the next Section.

10. Physical experiments

Our design method relies on simulating the geometric patterns with different configurations of loads and constraints, but we need to check the actual behavior of a physical structure with the aim of validating the accuracy of our design-to-fabrication pipeline. For a qualitative and quantitative assessment of our method, we fabricate and assemble a set of four physical objects, a sphere and three strips, using either uniform or variable pattern tessellations.

10.1. Fabrication results: qualitative evaluation

Our patterns can be assembled to create diverse surface tessellations. In a direct design fashion, the patterns can be selected from the design interface based on their aesthetics and stiffness.

Fig. 18(left) shows the first fabricated specimen. We adopt a truncated icosahedron geometry made of 20 regular hexagons and 12 regular pentagons to form a spherical surface. The purpose is to demonstrate the validity of our approach in the generation of patterns for different polygons and their tileability property. In general, if the polygon is as regular as possible, the structural simulations are valid in relative terms even if the number of polygon edges changes. Therefore, using different polygons as singularities has a negligible effect on the overall shape. In the present case, we select two patterns from the dome scenario with similar strain energy producing, indeed, when jointed, a spherical shape without distortions. It is worth mentioning that the adopted geometry and the number of connections favorably introduce a strong geometric constraint. The patterns have a negligible in-plane strain, and all the deformation is necessarily achieved by bending.

The pattern stiffness is related to its strain energy. Since our simulations use a constant force for all patterns in a scenario, patterns with a smaller resulting strain energy are stiffer than patterns with a higher one. These latter have larger deformation. Recently built examples [37, 38] demonstrate that, when joining patterns with uniform stiffness, both the tributary internal energy and deformation are similar for a uniform loading; instead, when joining patterns with different stiffness, only the tributary internal energy is similar.

In our specimen in Fig. 18(right), we tile groups of six regular hexagons to form a patterned strip, and we provide pin restraints at the extreme to observe a cylinder-like deformation. To showcase this effect, we select four patterns from the scatter plot of the cylinder scenario (Fig. 15(c)) with decreasing strain energies (from left to right in the strip of Fig. 18: 34.20, 33.18, 20.29 and 15.47 MPa). As expected, the internal force is constant for equilibrium reasons, and consequently, stiffer patterns (on the right) are almost undeformed. The bending attitude grows, moving to the left as the groups of patterns are ordered from the stiffer to the softer. The result is a surface which bends asymmetrically. The 3D printed flat PLA patterns are regular hexagons of 3.6 cm edge and 0.2 cm thickness, i.e., having the same properties adopted for the simulations. All pattern interfaces are connected through a 3D printed sleeve providing full restraint so that the resulting deformation of the assembled specimen is uniquely provided by the patterns' bending capacity.

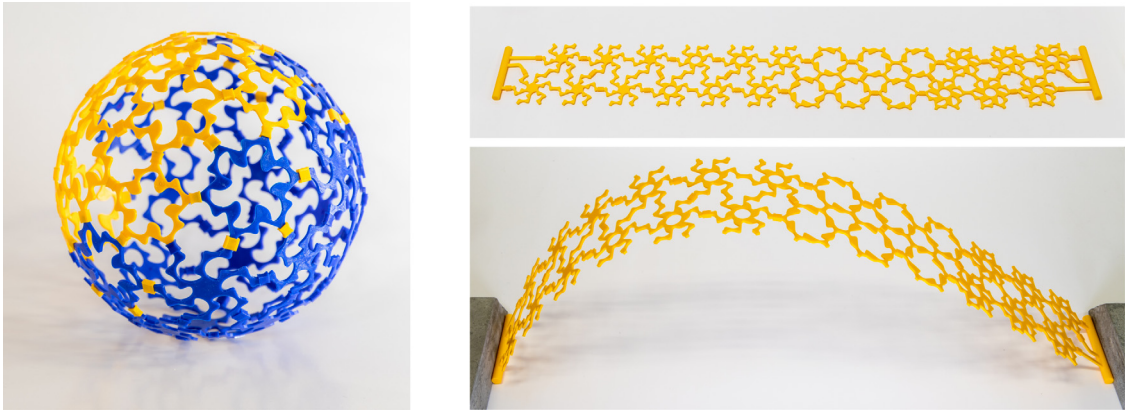

Fig. 18. Two fabricated examples to demonstrate the applicability of our method. (Left) a spherical assembly obtained by tessellating a truncated icosahedron using two patterns. (Right) a "graded" strip composed of four increasingly stiffer patterns (from left to right): when compressed horizontally the strip bends asymmetrically, accordingly with the employed pattern distribution.

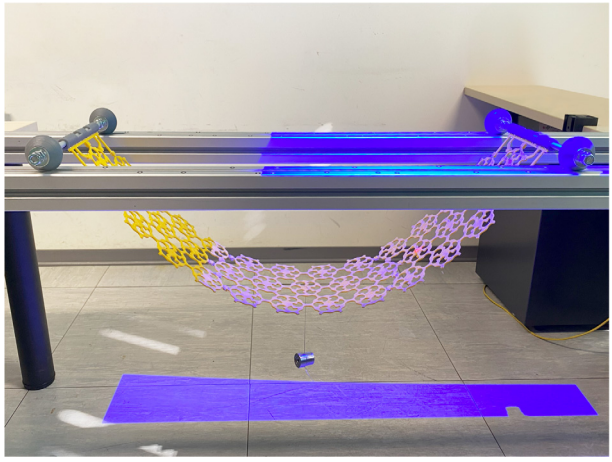

Fig. 19. Experimental setup for the test performed on the patterned specimen with an external load located at the center. The specimen deflects while the supports roll inward. At equilibrium, its shape is captured using a structured-light 3D scanner (gray 3D models in Fig. 20).

10.2. Fabrication results: quantitative evaluation

To measure the actual behavior of a tessellated structure under a load with respect to the simulation, we fabricate two assembled specimens, starting from selected patterns. We tile regular hexagons to form a 3×12 strip, with the central row having 13 hexagons. From the user interface, we select two patterns with different strain energy values, as depicted in Fig. 17(right). The green-highlighted pattern demonstrates higher strain energy, indicating greater bending capacity than the red-highlighted pattern. The first specimen is uniformly tiled with the red-highlighted pattern and is expected to exhibit an almost-uniform curvature. Conversely, the second specimen is tiled with two different patterns, one for each half. The expected curvature is higher on the half employing the softer pattern (green), while the other half specimen remains flatter due to the stiffer pattern adopted.

The two specimens are 3D printed using PLA material with a measured density of 1.81 g/cm^3, and a Young modulus of $E = 3.1$ GPa, taken from the producer's technical sheet (for the case of flat printing on the build plate). Due to the printer's working area, the specimens are printed in multiple sections and later joined using connectors.

The experimental setup is shown in Fig. 19. The extremes of the specimens are equipped with PLA connection profiles linking to free-rolling 8 mm aluminum shaft with almost-frictionless conic wheels that allow the translation along a rail. The total rest span is 843 mm. Two rigid 40×40 mm aluminum profiles with continuous grooves allow the specimen rollers to slide inward due to load. The test consists in suspending the specimens until the equilibrium is reached, measure their deflection via 3D scanning, and compare with the simulation results.

We test the specimens by affixing a weight of 70.5 g to the central pattern (Fig. 19). The specimens bend as a consequence of their own weight and the applied load: the deflected shape is then digitized using a metrology structured-light scanner (GOM ATOS 5M), using markers to ensure a precise data registration.

Fig. 20 shows the 3D models resulting from the 3D scanning (in gray) compared with a solid geometrically nonlinear simulation (colored) that adopts the same finite elements settings of Section 8, in front and perspective views. The 3D models are aligned to have a perfect overlap at the left support.

The uniformly tiled specimen (Fig. 20(top)) has a uniform stiffness and yields a deformed shape that tends to a catenary curve. The simulation well matches the overall shape measured with 3D scanning. The distance from the supports is 648.6 mm while the maximum deflection is 239.3 mm and is located at the center. However, the connectors linking the three sections slightly influence the real shape. Locally, they ensure geometric continuity but also cause stiffening. This effect is not modeled in the simulation; hence the distance between the two models results in 4.7 mm.

The two-patterns specimen (bottom in Fig. 20) has a more evident deformation, having a span 585.6 mm and maximum deflection 269.3 mm at equilibrium. Remarkably, as expected, it is affected by the uneven stiffness of the patterns, which makes the curvature higher on the left, where a slender pattern is used. Note that the right part is tiled with the same pattern of the first specimen. The lowest point of the deformed shape is indeed shifted on the left and occurs at the transition between patterns. The maximum distance between the 3D scanned model and the simulation is 4.6 mm.

11. Conclusions

This work focuses on the creation of a catalog of flat, tileable patterns to design mechanical metamaterials. Assuming a target surface approximated as a polygon mesh with (almost) regular faces, we define a regular recursive subdivision of polygons to produce exchangeable patterns to tile the surface. We define a strategy to filter the disconnected ones and conditions to ensure tileability. To produce geometries that are both fabricable and suited for simulations, we introduce a proper filleting strategy around non-manifold vertices, along with vertices that produce sharp angles, which could cause singularities in computation during mechanical simulations, and vertices that lie on the polygon boundary. We perform mechanical simulations of each pattern

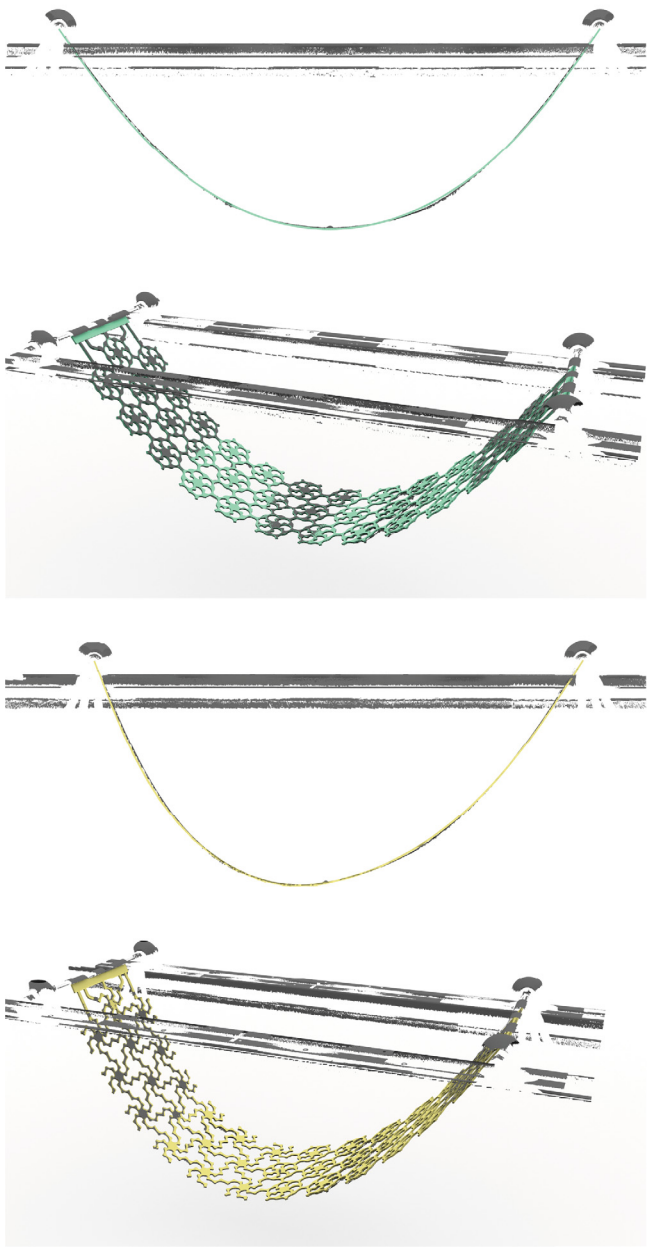

Fig. 20. 3D models measured in the experimental test (in gray) in comparison with a simulation based on finite elements (colored): at the top, the uniformly tiled specimen in front and perspective view; at the bottom, the two-patterns specimen in front and perspective view. The 3D scanner has measured only the top face of the specimens.

under three loading scenarios and implement a browsing interface that supports the exploration of the catalog of patterns in terms of aesthetics and mechanical behavior. Overall, significant variability in aesthetics and mechanical behavior is observed, also thanks to a strategy to produce continuous variations in the pattern geometries. Finally, we demonstrate that our patterns can be fabricated and assembled to create surface tessellations with different out-of-plane bending behavior. Our results, including the agreement between the physical experiments and the simulations, demonstrate the feasibility of our method as the first step in the direct design pipeline.

In the future, we plan to expand the browsing interface by including more aesthetic criteria for pattern selection, such as axial symmetry or the presence of a solid or empty center. We also plan to add the possibility to filter the patterns based on user-provided ranges of values for one or more criteria.

Besides addressing the direct design pipeline, future work could also include the inverse design problem, where the user provides a generic target shape. The most appropriate patterns are automatically selected and designed so that, once bent and assembled, they match the input shape. We believe that the seamless transition between the different patterns assembled in the fabricated sphere is a notable advantage in this direction, as it demonstrates that different patterns have the potential to integrate harmoniously within an assembled structure, without compromising the overall perception of the geometry.

A significant issue in conducting inverse design with metamaterials is that metamaterial structures present a complex geometry at the meso-scale, considerably increasing simulation costs. This reason pushed other researchers to work on simplified models, e.g. homogenization, thus severely limiting the design space. A possible research direction for finding equivalent metamaterial properties could be based on artificial intelligence techniques, with learned responses replacing computationally-intensive, physically-based simulations of the generic patterned surfaces.

Finally, a limitation of our approach is that it relies on an *a posteriori* filtering procedure of the generated patterns. In the future, we plan to study space-pruning strategies based on topological constraints that allow filtering at each step of recursion. This would orient the combinatorial exploration of the space of patterns towards a family of geometries that meet the constraints from the earlier steps.

CRediT authorship contribution statement

Elena Scandurra: Writing – original draft, Software, Methodology, Investigation, Data curation. **Francesco Laccone:** Writing – review & editing, Writing – original draft, Visualization, Validation, Supervision, Software, Resources, Methodology, Investigation, Data curation, Conceptualization. **Luigi Malomo:** Writing – review & editing, Writing – original draft, Visualization, Validation, Supervision, Software, Resources, Methodology, Investigation, Data curation, Conceptualization. **Marco Callieri:** Writing – review & editing, Validation, Supervision, Resources, Investigation, Data curation. **Paolo Cignoni:** Supervision, Resources, Project administration, Funding acquisition, Conceptualization. **Daniela Giorgi:** Writing – review & editing, Writing – original draft, Visualization, Validation, Supervision, Software, Resources, Project administration, Methodology, Investigation, Funding acquisition, Formal analysis, Data curation, Conceptualization.

Declaration of competing interest

The authors declare that they have no known competing financial interests or personal relationships that could have appeared to influence the work reported in this paper.

Data availability

Data will be made available on request.

Acknowledgments

This work was partially supported by the NextGenerationEU programme under the funding schemes PNRR-PE-AI scheme (M4C2, investment 1.3, line on AI) FAIR (Future Artificial Intelligence Research).

This paper has received financial support by the Horizon Europe Research & Innovation Programme under Grant agreement N. 101092612 (Social and hUman ceNtered XR - SUN project). Views and opinions expressed in this paper are those of the author(s) only and do not necessarily reflect those of the European Union. Neither the European Union nor the European Commission can be held responsible for them.

The authors gratefully thank Gianpaolo Palma for the support in preparing the specimens and the test rig.

References

[1] Bickel B, Bächer M, Otaduy MA, Lee HR, Pfister H, Gross M, et al. Design and fabrication of materials with desired deformation behavior. ACM Trans Graph 2010;29(4):1–10. http://dx.doi.org/10.1145/1778765.1778800.

[2] Panetta J, Zhou Q, Malomo L, Pietroni N, Cignoni P, Zorin D. Elastic textures for additive fabrication. ACM Trans Graph 2015;34(4):1–12. http://dx.doi.org/10.1145/2766937.

[3] Martínez J, Skouras M, Schumacher C, Hornus S, Lefebvre S, Thomaszewski B. Star-shaped metrics for mechanical metamaterial design. ACM Trans Graph 2019;38(4):1–13. http://dx.doi.org/10.1145/3306346.3322989.

[4] Pietroni N, Tonelli D, Puppo E, Froli M, Scopigno R, Cignoni P. Statics aware grid shells. Comput Graph Forum 2015;34(2):627–41. http://dx.doi.org/10.1111/cgf.12590.

[5] Scandurra E, Laccone F, Malomo L, Callieri M, Cignoni P, Giorgi D. Computational design of fabricable geometric patterns. In: Banterle F, Caggianese G, Capece N, Erra U, Lupinetti K, Manfredi G, editors. Smart tools and applications in graphics - eurographics Italian chapter conference. The Eurographics Association; 2023, http://dx.doi.org/10.2312/stag.20231297.

[6] Kaplan CS. Introductory tiling theory for computer graphics. Synth Lect Comput Graph Animat 2009;4(1):1–113.

[7] Grunbaum B, Shephard GC. Tilings and patterns. W. H. Freeman and Company; 1987.

[8] Pottmann H, Huang Q, Deng B, Schiftner A, Kilian M, Guibas L, et al. Geodesic patterns. ACM Trans Graph 2010;29(4). http://dx.doi.org/10.1145/1778765.1778780.

[9] Jiang C, Tang C, Vaxman A, Wonka P, Pottmann H. Polyhedral patterns. ACM Trans Graph 2015;34(6). http://dx.doi.org/10.1145/2816795.2818077.

[10] Santoni C, Pellacini F. gTangle: a grammar for the procedural generation of tangle patterns. ACM Trans Graph 2016;35(6). http://dx.doi.org/10.1145/2980179.2982417.

[11] Zhou S, Jiang C, Lefebvre S. Topology-constrained synthesis of vector patterns. ACM Trans Graph 2014;33(6). http://dx.doi.org/10.1145/2661229.2661238.

[12] Zehnder J, Coros S, Thomaszewski B. Designing structurally-sound ornamental curve networks. ACM Trans Graph 2016;35(4). http://dx.doi.org/10.1145/2897824.2925888.

[13] Chen W, Ma Y, Lefebvre S, Xin S, Martínez J, Wang W. Fabricable tile decors. ACM Trans Graph 2017;36(6). http://dx.doi.org/10.1145/3130800.3130817.

[14] Bickel B, Cignoni P, Malomo L, Pietroni N. State of the art on stylized fabrication. Comput Graph Forum 2018;37. http://dx.doi.org/10.1111/cgf.13327.

[15] Zehnder J, Coros S, Thomaszewski B. Designing structurally-sound ornamental curve networks. ACM Trans Graph 2016;35(4). http://dx.doi.org/10.1145/2897824.2925888.

[16] Schumacher C, Thomaszewski B, Gross M. Stenciling: Designing structurally-sound surfaces with decorative patterns. Comput Graph Forum 2016;35(5):101–10. http://dx.doi.org/10.1111/cgf.12967.

[17] Montes Maestre JS, Du Y, Hinchet R, Coros S, Thomaszewski B. Differentiable stripe patterns for inverse design of structured surfaces. ACM Trans Graph 2023;42(4). http://dx.doi.org/10.1145/3592114.

[18] Choi GPT, Dudte LH, Mahadevan L. Programming shape using kirigami tessellations. Nat Mater 2019;18(9):999–1004. http://dx.doi.org/10.1038/s41563-019-0452-y.

[19] Barchiesi E, Spagnuolo M, Placidi L. Mechanical metamaterials: a state of the art. Math Mech Solids 2019;24(1):212–34. http://dx.doi.org/10.1177/1081286517735695.

[20] Yu X, Zhou J, Liang H, Jiang Z, Wu L. Mechanical metamaterials associated with stiffness, rigidity and compressibility: A brief review. Prog Mater Sci 2018;94:114–73. http://dx.doi.org/10.1016/j.pmatsci.2017.12.003.

[21] Chen T, Panetta J, Schnaubelt M, Pauly M. Bistable auxetic surface structures. ACM Trans Graph 2021;40(4). http://dx.doi.org/10.1145/3450626.3459940.

[22] Ou J, Ma Z, Peters J, Dai S, Vlavianos N, Ishii H. KinetiX - designing auxetic-inspired deformable material structures. Comput Graph 2018;75:72–81. http://dx.doi.org/10.1016/j.cag.2018.06.003.

[23] Schumacher C, Bickel B, Rys J, Marschner S, Daraio C, Gross M. Microstructures to control elasticity in 3D printing. ACM Trans Graph 2015;34(4). http://dx.doi.org/10.1145/2766926.

[24] Guseinov R, McMahan C, Pérez J, Daraio C, Bickel B. Programming temporal morphing of self-actuated shells. Nat Commun 2020;11(1):237. http://dx.doi.org/10.1038/s41467-019-14015-2.

[25] Zhou Q, Panetta J, Zorin D. Worst-case structural analysis. ACM Trans Graph 2013;32(4). http://dx.doi.org/10.1145/2461912.2461967.

[26] Panetta J, Rahimian A, Zorin D. Worst-case stress relief for microstructures. ACM Trans Graph 2017;36(4). http://dx.doi.org/10.1145/3072959.3073649.

[27] Dumas J, Lu A, Lefebvre S, Wu J, Dick C. By-Example Synthesis of Structurally Sound Patterns. ACM Trans Graph 2015;34(4). http://dx.doi.org/10.1145/2766984.

[28] Martínez J, Dumas J, Lefebvre S, Wei L-Y. Structure and Appearance Optimization for Controllable Shape Design. ACM Trans Graph 2015;34(6). http://dx.doi.org/10.1145/2816795.2818101.

[29] Makatura L, Wang B, Chen Y-L, Deng B, Wojtan C, Bickel B, et al. Procedural metamaterials: A unified procedural graph for metamaterial design. ACM Trans Graph 2023;42(5). http://dx.doi.org/10.1145/3605389.

[30] Lee D, Chen WW, Wang L, Chan Y-C, Chen W. Data-driven design for metamaterials and multiscale systems: A review. Adv Mater 2023;2305254:2305254. http://dx.doi.org/10.1002/adma.202305254.

[31] Zhang Z, Brandt C, Jouve J, Wang Y, Chen T, Pauly M, et al. Computational design of flexible planar microstructures. ACM Trans Graph 2023;42(6). http://dx.doi.org/10.1145/3618396.

[32] Leimer K, Musialski P. Analysis of a reduced-order model for the simulation of elastic geometric zigzag-spring meta-materials. Comput Graph 2022;102:187–98. http://dx.doi.org/10.1016/j.cag.2021.10.007.

[33] Manolas I, Laccone F, Cherchi G, Malomo L, Cignoni P. Automated generation of flat tileable patterns and 3D reduced model simulation. Comput Graph 2022;106:141–51. http://dx.doi.org/10.1016/j.cag.2022.05.020.

[34] Sigmund O, Maute K. Topology optimization approaches: A comparative review. Struct Multidiscipl Optim 2013;48(6):1031–55. http://dx.doi.org/10.1007/s00158-013-0978-6.

[35] Huang X, Radman A, Xie YM. Topological design of microstructures of cellular materials for maximum bulk or shear modulus. Comput Mater Sci 2011;50(6):1861–70. http://dx.doi.org/10.1016/j.commatsci.2011.01.030.

[36] Lu H, Ting-Uei L, Ma J, Xie YM. Design optimisation of structures made of a small number of prescribed building blocks. Eng Struct 2024;304:117686. http://dx.doi.org/10.1016/j.engstruct.2024.117686.

[37] Malomo L, Pérez J, Iarussi E, Pietroni N, Miguel E, Cignoni P, et al. FlexMaps: Computational design of flat flexible shells for shaping 3D objects. ACM Trans Graph 2018;37(6). http://dx.doi.org/10.1145/3272127.3275076.

[38] Laccone F, Malomo L, Callieri M, Alderighi T, Muntoni A, Ponchio F, et al. Design and construction of a bending-active plywood structure: The flexmaps pavilion. J Int Assoc Shell and Spatial Struct 2022;63(2):98–114. http://dx.doi.org/10.20898/j.iass.2022.007.

[39] Laccone F, Malomo L, Pietroni N, Cignoni P, Schork T. Integrated computational framework for the design and fabrication of bending-active structures made from flat sheet material. Structures 2021;34:979–94. http://dx.doi.org/10.1016/j.istruc.2021.08.004.

[40] Tozoni DC, Dumas J, Jiang Z, Panetta J, Panozzo D, Zorin D. A low-parametric rhombic microstructure family for irregular lattices. ACM Trans Graph 2020;39(4). http://dx.doi.org/10.1145/3386569.3392451.

[41] Kharevych L, Mullen P, Owhadi H, Desbrun M. Numerical coarsening of inhomogeneous elastic materials. ACM Trans Graph 2009;28(3). http://dx.doi.org/10.1145/1531326.1531357.

[42] Schumacher C, Marschner S, Gross M, Thomaszewski B. Mechanical characterization of structured sheet materials. ACM Trans Graph 2018;37(4):1–15. http://dx.doi.org/10.1145/3197517.3201278.

[43] Šír Z, Jüttler B. On de casteljau-type algorithms for rational Bézier curves. J Comput Appl Math 2015;288:244–50. http://dx.doi.org/10.1016/j.cam.2015.01.037.

[44] Jacobson A, Panozzo D, et al. libigl: A simple C++ geometry processing library. 2018, https://libigl.github.io/.

[45] Muntoni A, Cignoni P. PyMeshLab. 2021, http://dx.doi.org/10.5281/zenodo.4438750.

[46] Smith M. ABAQUS/standard user's manual, version 6.9. United States: Dassault Systèmes Simulia Corp; 2009.